Bending mode fluctuations and structural stability of graphene nanoribbons

P. Scuracchio and A. Dobry

Facultad de Ciencias Exactas Ingeniería y Agrimensura, Universidad Nacional de Rosario and Instituto de Física Rosario, Bv. 27 de Febrero 210 bis, 2000 Rosario, Argentina

(Received 19 December 2012; published 5 April 2013)

We analyze the thermal fluctuations of a narrow graphene nanoribbon. Using a continuum membranelike model in the harmonic approximation, we study the height-height correlation functions and the destabilization modes corresponding to two different boundary conditions: fixed and free edges. For the first case, the thermal spectrum has a gap and the correlations along the ribbon decay exponentially. Thermal fluctuations produce only local perturbations of the flat situation. However, the long range crystalline order is not distorted. For free edges the situation changes as thermal excitations are gapless. The low energy spectrum decouples into a bulk and an edge excitation. The bulk excitation tends to destabilize the crystalline order producing a homogeneous rippling. Furthermore, we can relate the edge mode to a precluding perturbation leading to scrolled edges, as seen in suspended graphene samples. We also analyze the implications of our results in the thermal conductivity of graphene nanoribbons.

DOI: 10.1103/PhysRevB.87.165411 PACS number(s): 61.48.Gh, 63.22.Rc, 81.07.Bc

I. INTRODUCTION

The interplay between lattice deformations and electron dynamics is an important ingredient to take into account in order to understand and control the electronic properties of future graphene devices. On one side, an external strain applied to graphene produces a pseudomagnetic field whose effect was first predicted theoretically[1] and then determined experimentally.[2] This could be the starting point of a field called straintronics, namely the control of the electronic properties by applying mechanical strain. On the other hand, the intrinsic corrugation observed since the early experiments in suspended graphene samples affects the electron mobility. Fluctuations over this corrugation, called flexural phonons, have been proposed to be the source of the intrinsic limit in the electron mobility[3] and, certainly, the control of these corrugations is an important point to address.

When the dimensionality is reduced, height fluctuations are amplified due to the known tendency to instabilities in low dimensions. We expect thick ribbons with quasi-one-dimensional geometry to have stronger thermal fluctuations than two-dimensional systems. These fluctuations can have important effects on the electronic transport and the mechanism should be identified in order to control and manage the electronic properties of graphene nanoribbons.

The goal of the present paper is to study thermal excitations in graphene nanoribbons. We take a continuum model as a starting point, allowing us to account for the long-wavelength acoustic phonons. Our focus is to understand how the vibrational modes are affected by different boundary conditions and how these vibrations affect the static flat case. We analyze these points by calculating the out-of-plane flexural phonons and the height-height correlation functions for two different situations: clamped and free edges.

Phonon thermal conductivity plays an exciting role in graphene physics. Measurements[4] show that graphene could be one of the best heat conductors ever known, with thermal conductivity K as high as 5000 W/mK at room temperature in suspended samples. These results may open up new applications for thermal control in nanoelectronics. Moreover, the experimental values for K are not coincident,[5] and there is no agreement on what kind of phonons (in-plane or out-of-plane) produce the dominant contribution to K.[6] Our study could shed light on the role of the bending modes in graphene nanoribbons. We will discuss this point in the next sections.

This paper is organized as follows: In Sec. II we introduce the Hamiltonian model by taking a continuum limit of a tethered surface with bending energy. We also discuss how the appropriate boundary conditions can be taken into account. In Sec. III we present a general formalism based on a path integral to obtain the correlation functions. In Secs. IV and V we obtain the out-of-plane phononic spectrum and the correlation functions, analyzing their consequences. Finally, in Sec. VI we give our conclusions and perspectives.

II. THE MODEL AND THE BOUNDARY CONDITIONS

Single- and few-layer graphene are systems of atomic-scale thickness. As such, a continuum elastic theory for thick plates cannot be used straightforwardly. However, their mechanical properties, the formation of ripples, and the phonon spectrum as the basis of the electron-phonon interaction, are well described by the elastic energy form of thick plates. The clue to understanding this fact is that the bending rigidity in graphene does not arise from compressions and dilations of the continuum medium bounded by free surfaces. Therefore, the bending rigidity parameter cannot be obtained from the elastic parameters of the medium; instead, it is an independent quantity.[7] It is thought that the bending rigidity in graphene is due to the bond-angle and bond-order terms associated with the dihedral angles of the underlying C-C interactions.[8]

This distinction has a special significance in the presence of edges, as the case of the ribbons that we consider in this work. To make the discussion concrete, we start from a simplified tethered surface with bending energy, which has been introduced in the studies of membranes.[9] The model Hamiltonian is

$$E_{\text{bend}} = -\bar{\kappa} \sum_{\langle i,j \rangle} (\mathbf{n}_i \cdot \mathbf{n}_j - 1), \tag{1}$$

where $\mathbf{n}_i$ is the normal unit vector at the ith site of the lattice and j is its nearest neighbor. We use $\bar{\kappa}$ as the bending rigidity parameter in the lattice model. For small deviations from the flat configuration, we can parametrize the position of a point on the surface as

$$\mathbf{r}(x,y) = [x,y,h(x,y)]. \tag{2}$$

This is called Monge representation. $h(x,y)$ is the height variable and the normal unit vector can be calculated as

$$\mathbf{n}(x,y) = \frac{\mathbf{e}_z - \nabla h}{\sqrt{1+(\nabla h)^2}} = \frac{(-\partial_x h, -\partial_y h, 1)}{\sqrt{1+(\nabla h)^2}}, \tag{3}$$

where $\mathbf{e}_z$ is the unit vector in the z direction. Replacing this last expression in Eq. (1) and taking a continuum limit we obtain

$$\begin{aligned} H_{\text{bend}} &= \lim_{\text{cont}} \bar{\kappa} \sum_{\langle i,j\rangle} (1 - \mathbf{n}_i \cdot \mathbf{n}_j) = \lim_{\text{cont}} \frac{\bar{\kappa}}{2} \sum_{\langle i,j\rangle} (\mathbf{n}_i - \mathbf{n}_j)^2 \\ &= \frac{\kappa}{2} \int d^2x \left[\left(\partial_x^2 h\right)^2 + \left(\partial_y^2 h\right)^2 + 2(\partial_x \partial_y h)^2 \right]. \end{aligned} \tag{4}$$

Here $\kappa \propto \bar{\kappa}$[9,10] and we have kept terms up to order of $O(h^2)$. This is precisely the harmonic approximation of the bending Hamiltonian in terms of $h(x,y)$. One can see the explicit geometric contributions of Eq. (4) if we write it down in the following way:

$$H_{\text{bend}} = \frac{\kappa}{2} \int d^2x [(\nabla^2 h)^2 - 2\text{Det}(\partial_i \partial_j h)]. \tag{5}$$

The first term is proportional to the square of the mean curvature and the last one to the Gaussian curvature, both written in the harmonic approximation. In terms of these curvatures, Eq. (5) is known as the Helfrich form of the bending energy of a liquid membrane.[11] In particular, the Gaussian curvature is a total derivative term which has been neglected in previous studies on the stability of graphene membranes. However, it plays an important role in the search for the appropriate boundary conditions of our ribbon geometry.

If, instead of Eq. (1), we had begun with the elasticity problem of a thin plate, the bending energy would have assumed the same expression as Eq. (5).[12] However, in this last case, the bending rigidity would not be an independent parameter but a function of the elastic modulus of the plate as $\kappa = \frac{Yl^3}{12(1-\sigma^2)}$, with l its thickness, Y is the Young's modulus, and σ is the Poisson ratio. Also, the Gaussian curvature in the second term of Eq. (5) would be multiplied by $(1-\sigma)$. Regarding the discussion at the beginning of this section, we see that there is a formal connection between the theory of thin elastic plates and the one of two-dimensional membranes. The last one can be obtained from the other one by taking the bending rigidity as an independent parameter and by setting $\sigma = 0$.

When expressing $(\nabla^2 h)^2$ in the form of hOh, we find another total derivative term. Then, Eq. (5) can be written as

$$\begin{aligned} H_{\text{bend}} = \frac{\kappa}{2} \int d^2x \big[& h\left(\partial_x^4 + \partial_y^4 + 2\partial_x^2 \partial_y^2\right) h \\ & + \partial_x \left(\partial_x h \partial_x^2 h - h \partial_x^3 h - 2h \partial_y^2 \partial_x h\right) \\ & + \partial_y \left(\partial_y h \partial_y^2 h - h \partial_y^3 h + 2\partial_x h \partial_y \partial_x h\right) \big]. \end{aligned} \tag{6}$$

Until now we have not specified the integration domain and the physical boundary conditions for our problem. We consider a long and narrow ribbon of width W and length L running along the y direction. The domain of integration is therefore given by $-W/2 \leqslant x \leqslant W/2$ and $-L/2 \leqslant y \leqslant L/2$ with $W \ll L$. We use periodic boundary conditions in the y direction. Therefore, the surface term corresponding to the last line of Eq. (6) vanishes. Finally, we obtain the following bending energy for the ribbon:

$$\begin{aligned} H_{\text{bend}} = \frac{\kappa}{2} & \int_{-\frac{L}{2}}^{\frac{L}{2}} dy \int_{-\frac{W}{2}}^{\frac{W}{2}} dx \left[h\left(\partial_x^4 + \partial_y^4 + 2\partial_x^2 \partial_y^2\right) h \right] \\ & + \int_{-\frac{L}{2}}^{\frac{L}{2}} dy \left\{ \partial_x h(x,y) \left[\partial_x^2 h(x,y) \right] \right. \\ & \left. - h(x,y) \left[\partial_x^3 h(x,y) + 2\partial_y^2 \partial_x h(x,y) \right] \right\}_{x=\pm W/2}, \end{aligned} \tag{7}$$

where the last symbol means that the term in braces is the difference between this expression evaluated at $x = \frac{W}{2}$ and at $x = -\frac{W}{2}$. Therefore, the integral runs along the edges of the ribbon. A cancellation of this term could take place in two different situations. Consider a ribbon with clamped edges along the y direction. In this case we have

$$h\left(x = \pm\frac{W}{2}, y\right) = 0, \quad \partial_x h\left(x = \pm\frac{W}{2}, y\right) = 0. \tag{8}$$

The terms multiplying $h(x = \pm\frac{W}{2}, y)$ and $\partial_x h(x = \pm\frac{W}{2}, y)$ can be interpreted as the force and the torque on the edge of the ribbon.[12] Setting these terms to zero means having free edges, and the boundary conditions are then

$$\begin{aligned} \left(\partial_x^3 + 2\partial_y^2 \partial_x\right) h\left(x = \pm\frac{W}{2}, y\right) = 0, \\ \partial_x^2 h\left(x = \pm\frac{W}{2}, y\right) = 0. \end{aligned} \tag{9}$$

Note that those are the situations (clamped and free) considered in Ref. 13 to obtain the phonon dispersion relation of a nanoribbon. In this reference, the theory of an elastic thin plate is used instead and the following boundary conditions are considered for free edges:

$$\begin{aligned} \left[\partial_x^3 + (2-\sigma)\partial_y^2 \partial_x\right] h\left(x = \pm\frac{W}{2}, y\right) = 0, \\ \left(\partial_x^2 + \sigma \partial_y^2\right) h\left(x = \pm\frac{W}{2}, y\right) = 0. \end{aligned} \tag{10}$$

For $\sigma = 0$, Eq. (10) is the same as Eq. (9) as we already remarked. So far we have not discussed about the elastic stretching energy of the ribbon. This is because, in the harmonic approximation, the in-plane modes that correspond to the stretching energy are decoupled from the out-of-plane ones, allowing us to study these situations separately. In the next section we will compare the height-height correlation function and the mean square of the height corresponding to the two different boundary conditions given by Eqs. (8) and (9).

III. GENERAL FORMALISM FOR CORRELATION FUNCTIONS

For both clamped and free boundaries, the surface term in Eq. (6) vanishes, and the partition function of the system can be written as a path integral of the form

$$Z = \int \mathcal{D}h \exp\left\{-\frac{\kappa}{2kT}\int_{-\frac{L}{2}}^{\frac{L}{2}} dy \times \int_{-\frac{W}{2}}^{\frac{W}{2}} dx\left[h\underbrace{\left(\partial_x^4+\partial_y^4+2\partial_x^2\partial_y^2\right)}_{O} h\right]\right\}, \quad (11)$$

integrating over all the paths that fulfill the boundary conditions (8) or (9). It is convenient to expand the path in the basis of the eigenfunctions of the operator O. Due to the periodic boundary condition in the long direction, we can separate its y dependence. The eigenfunctions assume the form $f_m^n(x)e^{iq_m y}$, where $q_m = \frac{2\pi m}{L}$, and f_m^n are the eigenfunctions of the following problem:

$$\left[q_m^4 + \partial_x^4 - 2q_m^2\partial_x^2\right] f_m^n(x) = \lambda_{m,n}^2\, f_m^n(x). \quad (12)$$

This situation is quite similar to the one analyzed in Ref. 13 to solve the classical dynamics for the out-of-plane normal modes. We define the dimensionless variables $\bar{q}_m = W q_m$, $\bar{\lambda} = \lambda W^2$, $\bar{x} = \frac{x}{W}$, and $\bar{y} = \frac{y}{W}$. The solutions of Eq. (12) can be written as

$$f_m^n(\bar{x}) = \sum_{i=1}^{4} d_i\, e^{\beta_i \bar{x}}, \quad (13)$$

with

$$\beta_i(m,n) = \pm\sqrt{\bar{q}_m^2 \pm \bar{\lambda}_{m,n}}. \quad (14)$$

After replacing Eq. (13) in the boundary conditions (8) or (9) we obtain a linear 4×4 problem whose solutions give $\bar{\lambda}$ as a function of $\bar{q}$, and the coefficients d_i to construct the normalized eigenfunctions. We will elaborate on this route in the next section.

Once we have solved this problem, the expression for $h(x,y)$ can be expanded as

$$\bar{h}(\bar{x},\bar{y}) = \sum_{m,n} \alpha_{m,n}\, f_m^n(\bar{x})\, e^{i\bar{q}_m\bar{y}}, \quad (15)$$

where $\bar{h}(\bar{x},\bar{y}) \equiv \frac{h(W\bar{x},W\bar{y})}{W}$. Applying the corresponding change of variables, the path integral (11) will run now on the coefficients $\alpha_{m,n}$ and the height-height correlation function $\langle\bar{h}(\bar{x}_1,\bar{y}_1)\bar{h}(\bar{x}_2,\bar{y}_2)\rangle$ can be obtained as usual by adding a source term of the form $\sum\alpha_{m,n}\epsilon_{m,n}$ to the exponent and then taking the derivative with respect to $\epsilon_{m,n}$. The result is

$$\langle\bar{h}(\bar{x}_1,\bar{y}_1)\bar{h}(\bar{x}_2,\bar{y}_2)\rangle = \frac{kT}{\kappa\bar{L}}\sum_{m,n} e^{i(\bar{y}_1-\bar{y}_2)\bar{q}_m}\frac{f_m^n(\bar{x}_1)f_m^n(\bar{x}_2)}{\bar{\lambda}_{m,n}^2}. \quad (16)$$

In the previous equation we assumed that the eigenfunctions are normalized in such a way that $\int_{-\frac{1}{2}}^{\frac{1}{2}}|f_m^n(\bar{x})|^2 d\bar{x} = 1$.

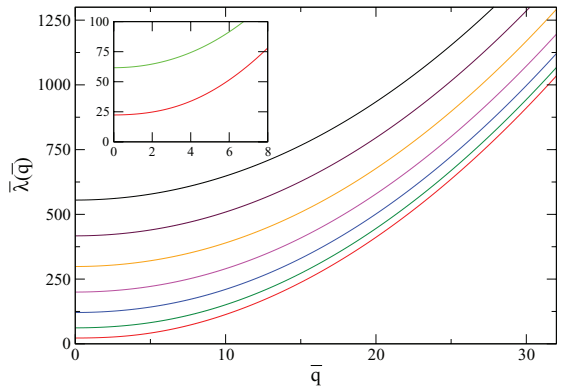

FIG. 1. (Color online) Dispersion curves given by the functions $\bar{\lambda}(\bar{q})$ for the clamped ribbon. We show the first seven branches of the spectrum which, in fact, has an infinite number of them. In the inset we show a zoom of the low energy spectrum for the first two branches.

IV. CORRELATION FUNCTIONS FOR CLAMPED RIBBONS

Imposing the conditions of Eq. (8) over $\bar{h}(\bar{x},\bar{y})$ expressed in terms of $f_m^n(\bar{x})$ according to Eq. (13), we obtain a 4×4 matrix $\mathcal{M}(\bar{\lambda},\bar{q})$ that multiplies the vector of coefficients (d_1,d_2,d_3,d_4), and whose result must be zero. Explicitly

$$\mathcal{M} = \begin{pmatrix} e^{\frac{a}{2}} & e^{-\frac{a}{2}} & \cos\left[\frac{b}{2}\right] & \sin\left[\frac{b}{2}\right] \\ e^{-\frac{a}{2}} & e^{\frac{a}{2}} & \cos\left[\frac{b}{2}\right] & -\sin\left[\frac{b}{2}\right] \\ a\, e^{\frac{a}{2}} & -a\, e^{-\frac{a}{2}} & -b\, \sin\left[\frac{b}{2}\right] & b\, \cos\left[\frac{b}{2}\right] \\ -a\, e^{-\frac{a}{2}} & a\, e^{\frac{a}{2}} & -b\, \sin\left[\frac{b}{2}\right] & -b\, \cos\left[\frac{b}{2}\right] \end{pmatrix}, \quad (17)$$

where $a = \sqrt{\bar{q}_m^2 + \bar{\lambda}_{m,n}}$ and $b = \sqrt{\bar{\lambda}_{m,n} - \bar{q}_m^2}$ are real variables. By requiring that $\mathrm{Det}[\mathcal{M}] = 0$ we obtain the values of $\bar{\lambda}_{m,n}$ for each $\bar{q}_m$. The index $n = 0, 1, 2, 3, \ldots$ used so far enumerates the dispersion curves, which are shown in Fig. 1. These boundary conditions allow us to simplify the determinant of the matrix $\mathcal{M}$, which can be factorized in two terms:

$$\mathrm{Det}[\mathcal{M}] = -8\left(a\,\cosh\left[\frac{a}{2}\right]\sin\left[\frac{b}{2}\right] - b\,\cos\left[\frac{b}{2}\right]\sinh\left[\frac{a}{2}\right]\right) \times \left(b\,\cosh\left[\frac{a}{2}\right]\sin\left[\frac{b}{2}\right] + a\,\cos\left[\frac{b}{2}\right]\sinh\left[\frac{a}{2}\right]\right). \quad (18)$$

Under these circumstances the matrix $\mathcal{M}$ is reduced to a simpler form and the eigenfunctions $f_m^n(\bar{x})$ can be calculated explicitly. When the first term vanishes, we obtain the $n = 1, 3, 5, \ldots$ branches of the spectrum with the odd eigenfunctions, which read

$$f_m^n(\bar{x}) = C_n\left(-\frac{\cos[b/2]}{\cosh[a/2]}\cosh[a\bar{x}] + \cos[b\bar{x}]\right), \quad (19)$$

and when the second term vanishes, we obtain the $n = 0, 2, 4, \ldots$ ones with the even eigenfunctions, which can be written as

$$f_m^n(\bar{x}) = C_n\left(-\frac{\sin[b/2]}{\sinh[a/2]}\sinh[a\bar{x}] + \sin[b\bar{x}]\right). \quad (20)$$

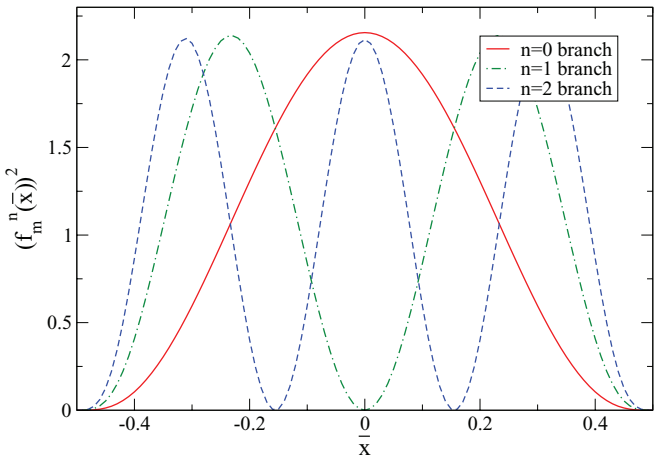

FIG. 2. (Color online) Square of the normalized eigenfunctions $f_m^n(\bar{x})$ for the first three branches of the spectrum in the clamped ribbon. These calculations are made for $\bar{q} = 6\pi$.

The quantities C_n, as remarked at the end of Sec. III, represent normalization constants. Plots for $(f_m^n(\bar{x}))^2$ with $n = 0, 1, 2$ and $\bar{q}_m = 6\pi$ are shown in Fig. 2. As pointed out in Ref. 13, there is a gap in the spectrum and the zero energy mode does not exist for $\bar{q}_m = 0$. This is related to the fact that global translations are not allowed because the ribbon is clamped at the edges. The gap in the first branch behaves as $\Delta \sim \frac{22.3}{W^2}$ (in the original units) approaching the zero value for the infinite square sheet. We expect the height-height correlations at different points to decay exponentially and this is indeed the case. In Fig. 3 we show the value of $\frac{\kappa}{kT}\langle\bar{h}(0.25,\bar{y})\bar{h}(0.25,0)\rangle$ running along the y direction and evaluated numerically from Eq. (16). The contribution from the first three branches is shown. As the gap increases we go to branches with higher energy, the contributions of the corresponding correlations become increasingly smaller. A fast decay of the correlations is observed in a distance of the order of W. In fact, we can estimate the characteristic correlation length with the

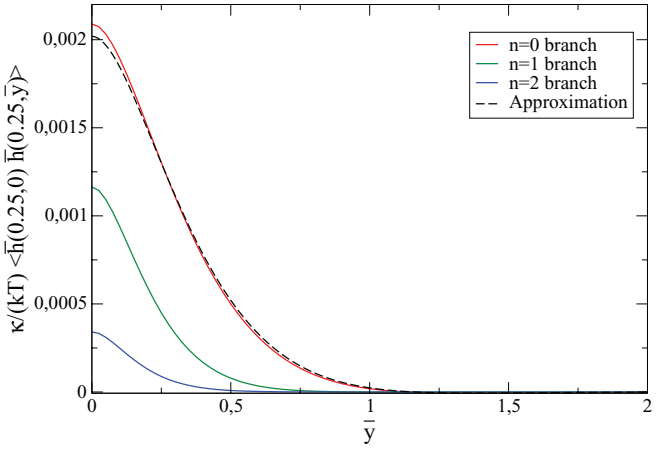

FIG. 3. (Color online) Height-height $\frac{\kappa}{kT}\langle\bar{h}(0.25,\bar{y})\bar{h}(0.25,0)\rangle$ correlation as a function of the distance in the long direction, for the clamped ribbon. The contributions of the three first branches are shown separately. The dashed line represents the approximation given by Eq. (22). The length of the ribbons is $L = 1000$ and its width $W = 100$.

following approximations. The first branch of Fig. 1 can be fitted by a function of the form $\bar{\lambda}_0(\bar{q}) \simeq \sqrt{a_0 + a_1\bar{q}^2 + a_2\bar{q}^4}$, with $a_0 = 500$, $a_1 = 24$, and $a_2 = 0.972$. If we neglect the weak dependency of the eigenfunctions on $\bar{q}_m$ in Eq. (16), the y dependency of the correlation is given by the following Fourier transform:

$$\langle\bar{h}(\bar{x}_1,\bar{y})\bar{h}(\bar{x}_2,0)\rangle \simeq f_m^0(\bar{x}_1)f_m^0(\bar{x}_2)\int_{-\infty}^{+\infty}\frac{d\bar{q}}{2\pi}\frac{e^{i\bar{q}\bar{y}}}{a_0 + a_1\bar{q}^2 + a_2\bar{q}^4}, \quad (21)$$

which can be solved analytically, giving

$$\langle\bar{h}(\bar{x}_1,\bar{y})\bar{h}(\bar{x}_2,0)\rangle \simeq f_m^0(\bar{x}_1)f_m^0(\bar{x}_2)e^{-q_I\bar{y}} \times [\alpha\sin(q_R\bar{y}) + \beta\cos(q_R\bar{y})], \quad (22)$$

where $\alpha = 0.00499$, $\beta = 0.00271$, and $q_R + iq_I = 2.273 + i4.185$ is a zero of the denominator of Eq. (21). The decay of the correlation is clearly dominated by the exponential term. Its characteristic scale, i.e., the correlation length, is $\xi = W/4.185$ (in the original units).

We see that it is possible to control the extension of the height-height correlation by changing the width of the ribbon. If we associate this thermal fluctuation with the rippling, these results imply that the characteristic size of the rippled region grows linearly with the width of the ribbons. In Fig. 4 we show the values of $\langle\bar{h}^2(\bar{x},\bar{y})\rangle$ for the first three branches of Fig. 1. The dominant contribution coming from the first branch produces a maximum distortion at the center of the ribbons. The other branches produce periodic distortions according to the shape of the eigenfunctions $f_m^n(\bar{x})$, as shown in Fig. 2. The number of nodes is exactly $n + 2$ including those at the edges.

Let us discuss the possible use of the previous results to clarify the relative contribution of the in-plane and flexural phonons on the intrinsic heat conductivity of graphene. The gap in the phonon spectrum for the clamped ribbons implies that, indeed, no acoustic phonons exist, which leads to a strong reduction of K. However, as shown in Ref. 13, this gap is actually very small for realistic values of W. In fact, for $W =$ 30 nm, the gap is $\Delta_{OP} = 7.9\ \mu$eV. As the translation symmetry

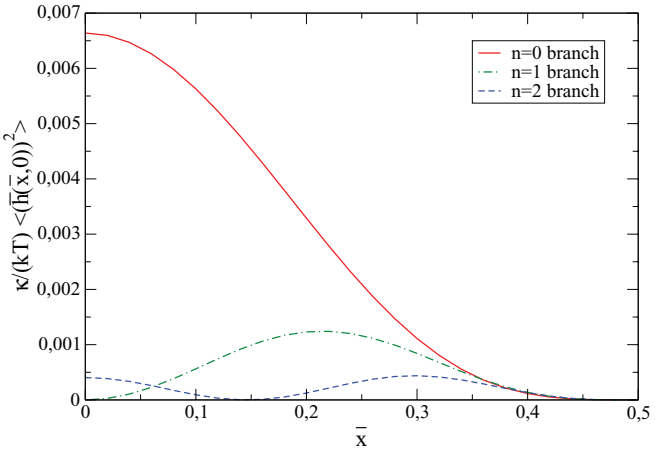

FIG. 4. (Color online) Mean square of the height $\frac{\kappa}{kT}\langle\bar{h}(\bar{x},\bar{y})^2\rangle$ as a function on $\bar{x}$, the distance to the center, for the clamped ribbon. We show the contributions of the first three branches. The length of the ribbons is $L = 1000$ and its width $W = 100$.

is broken in all directions, there is also a gap for the in-plane phonons. It has been estimated in Ref. 13 to be $\Delta_{IP} = 1$ meV for a ribbon of the same width, much higher than Δ_{OP}. For temperatures sufficiently lower than RT we expect the out-of-plane phonons to be excited but not the corresponding in-plane modes. If future determinations of $K(T)$ in clamped samples show a reduction at low temperature, we would conclude that these phonons are not quite relevant for thermal conductivity as claimed in previous works.[14]

V. CORRELATION FUNCTIONS AND STABILITY OF RIBBONS WITH FREE EDGES

In a recent paper[15] one of the authors studied the thermal fluctuations and the stability of a graphene ribbon with periodic boundary conditions in both directions, in order to avoid edge effects. It was found, from both analytical calculations and Monte Carlo simulations, that there is a critical relation between the width and the length of the system (called $R_{2D\text{-}1D}$) in which the dependence of $\langle \bar{h}^2(\bar{x},\bar{y})\rangle$ with the system size changes. When the width decreases and the relation with the length becomes smaller than $R_{2D\text{-}1D}$, thermal oscillations are more pronounced than in the opposite case. The system behaves as one-dimensional and there is a higher tendency to a crumpled instability than in square samples.

Moreover, the results of Ref. 15 (which include anharmonic terms) do not take into account possible excitations of the edges. To consider this kind of excitations in a more realistic description, we analyze the out-of-plane modes of a ribbon with free boundary conditions, as given by Eq. (9). Following similar steps as in the previous section, but with the corresponding boundary conditions, we obtain the dispersion relation of the out-of-plane modes which are shown in Fig. 5. Differently than in the clamped ribbon, as translational invariance is not broken, we find a gapless dispersion with two acoustic branches of zero energy at $\bar{q} = 0$. Qualitatively, we find a similar spectrum as the one in Ref. 13 where a finite Poisson ratio is considered and the boundary

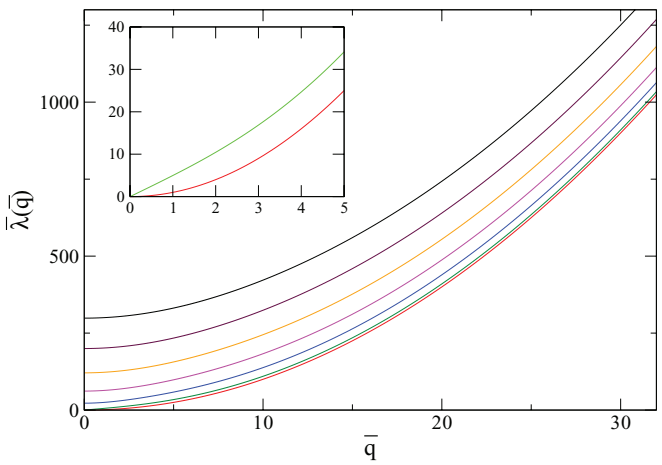

FIG. 5. (Color online) Dispersion relation giving the functions $\bar{\lambda}(\bar{q})$ for the free ribbon. We show the first seven branches of the spectrum. In the inset we show a zoom of the low energy spectrum for the two first branches.

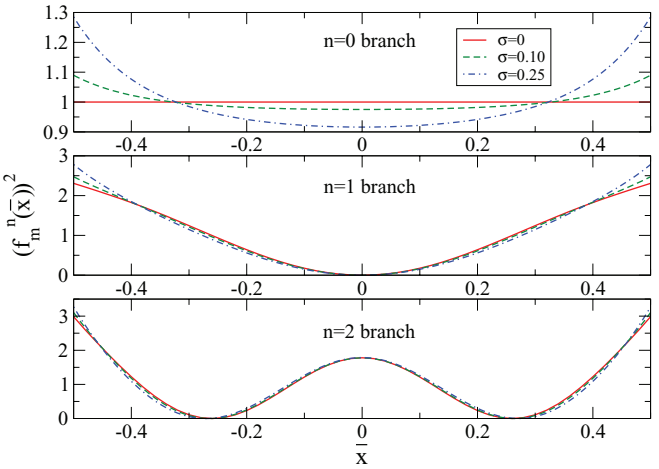

FIG. 6. (Color online) Square of the normalized eigenfunctions $f_n^m(\bar{x})$ corresponding to the first (upper panel), second (middle panel), and third branch (lower panel) of Fig. 5. We also show for comparison the square of eigenfunctions for ribbons with finite Poisson ratio $\sigma = 0.1$ and $\sigma = 0.25$.

conditions given by Eq. (10) are used. However, there are some important differences that appear with a careful inspection of the two lowest energy branches and their corresponding eigenfunctions. First of all, note that a function of the form $h(x,y) = Ce^{iqy}$, in which C is a constant, fulfills condition (9) but not (10). This is a solution of the eigenproblem(12) with a constant eigenfunction and dispersion relation $\bar{\lambda}(\bar{q}) = \bar{q}^2$, and this is precisely the eigenfunction corresponding to the lowest energy branch of a system with periodic boundary conditions in the x direction, as analyzed in Ref. 15. We identify this as a bulk mode, corresponding to the first branch in Fig. 5.

This is different than the situation we find when the boundary conditions given by Eq. (10) are used. For comparison, we show the square of the eigenfunctions corresponding to the first branch in the upper panel of Fig. 6 for different values of the Poisson ratio σ. We see that it is a constant function corresponding to a pure bulk mode only for $\sigma = 0$, when a two-dimensional membrane model is used. For finite values of σ the eigenfunctions depend on the position over the ribbon and do not represent a bulk mode anymore, otherwise the dispersion relation of the second branch could be fitted by a law $\bar{\lambda}(\bar{q}) = \bar{q}\sqrt{a_0 + a_1\bar{q}^2}$ which disperses linearly near $\bar{q} = 0$ and then quadratically for large values of $\bar{q}$. The square of the eigenfunctions corresponding to this mode are shown in the middle panel of Fig. 6. We see that the most important distortion occurs when we approach to the edges. This mode is therefore mostly an edge excitation and its behavior is qualitatively similar for both $\sigma = 0$ and $\sigma \neq 0$.

We arrive at an important conclusion: When a theory of a two-dimensional membrane is used, which we assume is the correct one for single- or few-layer graphene systems, the low energy phonon spectrum is decoupled into two branches with quite different physical interpretations. One corresponds to a bulk excitation and the other one is mainly an edge mode.

Let us explore the consequences for the mean square amplitude of the height $\langle \bar{h}^2(\bar{x},\bar{y})\rangle$. Differently than in clamped

ribbons, there are two gapless branches that give rise to a strong dependency with the length of the system $\sim L$ and a divergence when $L \to \infty$. This can be interpreted as an intrinsic instability of the system. However, it is known that the harmonic approximation is not valid for small values of $\bar{q}$, in which the anharmonic coupling between the in-plane and the out-of-plane modes[15,16] can stabilize the ribbon (or at least weaken the divergences). Moreover, the inclusion of external strains which are ubiquitous in real samples, will help to stabilize the system.[17]

One is tempted to connect this elastic instability with the possible divergence of the thermal conductivity in two-dimensional systems that has been widely debated in relation to graphene samples.[18,19] Furthermore, the elastic instability already appears in the harmonic approximation where the bending and in-plane modes are decoupled. An intrinsic size dependency analysis of K within our continuum model would necessarily include anharmonic terms which couple out and in-plane modes. This calculation could be conducted on the lines of the Appendix of Ref. 19 and deserves a separate study.

The physical effect of the distortion of the ribbon will be quite different depending on the contribution of each of the two lower energy branches. The first one, with quadratic dispersion relation, is a bulk mode. We expect the same effect as the one analyzed in Ref. 15, i.e., to produce an homogeneous rippling. More important for the goal of this paper is the effect of the second branch. In Fig. 7 we show the result for $\langle \bar{h}^2(\bar{x},\bar{y})\rangle$ calculated using the eigenvectors and eigenvalues corresponding to the second (upper panel) and the third (lower panel) branch of Fig. 5. As in the previous figure, we compare this result to ribbons with finite Poisson ratios $\sigma = 0.1$ and $\sigma = 0.25$. We see again that the maximum of $\langle \bar{h}^2(\bar{x},\bar{y})\rangle$ is at the boundary for each value of σ. Regarding the contribution of the third branch, the correlation is strongly reduced as there is a gap for these excitations. A minimum around $\bar{x} \sim 0.28$ is observed as well, corresponding to a node in the eigenfunctions. The height-height correlation function

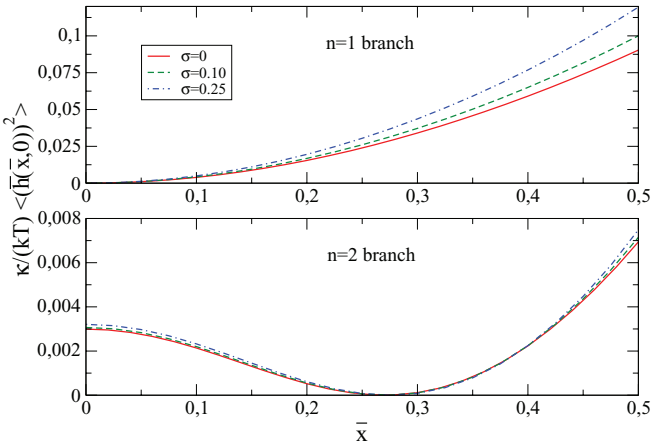

FIG. 7. (Color online) Correlation $\frac{\kappa}{kT}\langle \bar{h}^2(\bar{x},\bar{y})\rangle$ obtained with the eigenfunctions corresponding to the second branch (upper panel) and third branch (lower panel) of Fig. 5. We also show, for comparison, the corresponding quantities for a ribbon with finite Poisson ratios $\sigma = 0.1$ and $\sigma = 0.25$. The length of the ribbons is $L = 1000$ and its width $W = 100$.

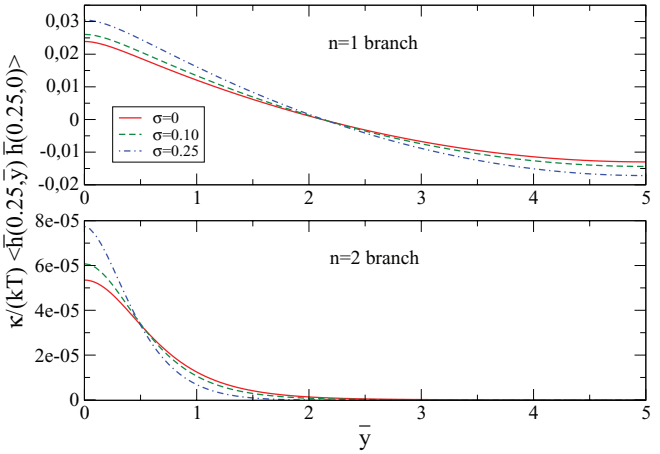

FIG. 8. (Color online) Correlation $\frac{\kappa}{kT}\langle h(0.25,0)h(0.25,y)\rangle$ obtained with the eigenfunctions and eigenvalues corresponding to the second branch (upper panel) and the third branch (lower panel) of Fig. 5. We also show, for comparison, the corresponding quantity for ribbons with finite Poisson ratios $\sigma = 0.1$ and $\sigma = 0.25$. The length of the ribbons is $L = 1000$ and its width $W = 100$.

is shown in Fig. 8 as a function of $\bar{y}$ for fixed $\bar{x} = 0.25$. Regarding the contribution of the third branch in the lower panel, its behavior is similar to the one seen in the clamped ribbon, as analyzed in the previous section. The correlation function has very small values and decays exponentially with the $\bar{y}$ distance. However, the contribution of the second branch is much more important and the correlation function decays much more slowly. This is a consequence of the absence of a gap for this mode. In fact, the value that this correlation assumes will increase with the length of the ribbon. Note that correlations in momentum space decay as $\propto \frac{1}{q^2}$ at small q. This may be compared with a 2D-infinite membrane, whose correlations behave as $\propto \frac{1}{q^4}$ and diverge more rapidly near $q = 0$ than the ones of the ribbons.

Finally, let us briefly discuss the consequence of this result for a distortion of a free standing sample. From early measurements it has been observed that when graphene samples are put in a scaffold configuration, the free edges appear folded.[20] The fact that a scrolled configuration can be a stable deformation of a graphene edge has been previously shown.[21] It is stabilized by an interplay between the van der Waals and bending energies. The edge modes we have found in the present paper could be interpreted as precursive modes for this highly distorted structure. That is to say, one possible sequence of events might be: First, the edge oscillates rapidly with increasing amplitude and second, it sticks to the rest of the sample due to the attractive van der Waals force.

VI. CONCLUSION AND DISCUSSION

In this paper we have studied the out-of-plane phononic spectrum and the height-height correlation functions of a graphene nanoribbon. Two different configurations were considered: clamped and free edges. When the ribbon is clamped, there are no true acoustic branches but a gap in the phononic spectrum. This gap leads to an exponential decay

of the correlations and thermal excitations produce only local distortions of the crystalline order. This looks quite similar to the situation in usual three-dimensional solids. However, when the lateral dimension W increases enough, the characteristic correlation length also increases. This is coherent with the fact that in a infinite square membrane, the height-height correlation decays as a power law.[16]

When the edges are free, we find quite a remarkable decoupling between two different low energy phononic branches. Both of them go to zero energy for $\bar{q} \to 0$ and one of them disperses quadratically for all values of $\bar{q}$. The eigenvectors associated to this branch do not depend on the transverse coordinate of the ribbon. Therefore, in these modes the system is unaware of the existence of edges. It is in fact a bulk excitation, similar to a lower excitation of an infinite membrane. The possible instability connected with this mode could lead the system to an homogeneous rippling. The other low energy branch disperses linearly for small values of $\bar{q}$. The corresponding eigenvectors have their maximum values at the edges. It is a surface or edge mode, and an instability is also associated with these modes. We claim that they could be the precursive modes resulting in folded edges as seen experimentally in suspended graphene samples.

We remark that this decoupling between a bulk and an edge mode is specific for a membranelike model. In a model for a continuum plate in which a finite thickness is assumed, both modes are essentially edge modes. This model could be relevant for other membranes made of conventional semiconductors.[22] For graphene, which is a one-atom thick sheet, the decoupling between an edge and a bulk mode will have a special significance. For instance, the presence of defects or disorder at the edges will affect mainly the edge modes but not the bulk ones.

The edge mode could play some role in the thermal conductivity. Indeed, the prediction that the bending modes would give a negligible contribution to K was related with its small group velocity and its large Umklapp scattering rate.[14] The edge mode has a linear dispersion relation and its group velocity increases with respect to the bulk modes. Even so, a complete study of the anharmonicities is necessary to give precise results, assuming the same scattering rate for the bulk and the edge modes, for which this last one should contribute more than the former to the thermal transport in graphene nanoribbons.

A possible extension of our work could be the study of interactions between the vibrational modes and the conducting electrons in nanoribbons. It has been shown that flexural phonons play an essential role as a limiting mechanism for the mobility in suspended graphene samples. We presume similar effects in nanoribbons. Moreover, when the edges of the ribbon are of zigzag type, localized electronic states near the edges are expected.[23] The phononic modes found in the present work should interact considerably with these confined electronic states. We expect them to have an important impact in the transport properties of these nanoribbons.

ACKNOWLEDGMENTS

We thank D. Mastrogiuseppe and S. Costamagna for usefull discussions. This work was partially supported by PIP 11220090100392 of CONICET, and PICT R 1776 of the ANPCyT.

[1] F. Guinea, M. I. Katsnelson, and A. K. Geim, Nat. Phys. **6**, 30 (2010).
[2] N. Levy, S. A. Burke, K. L. Meaker, M. Panlasigui, A. Zettl, F. Guinea, A. H. Castro Neto, and M. F. Crommie, Science **329**, 544 (2010).
[3] E. V. Castro, H. Ochoa, M. I. Katsnelson, R. V. Gorbachev, D. C. Elias, K. S. Novoselov, A. K. Geim, and F. Guinea, Phys. Rev. Lett. **105**, 266601 (2010).
[4] A. A. Balandin, S. Ghosh, W. Bao, I. Calizo, D. Teweldebrhan, F. Miao, and C. N. Lau, Nano Lett. **8**, 902 (2008).
[5] A. A. Balandin, Nat. Mater. **10**, 569 (2011).
[6] A. A. Balandin and D. L. Nika, Mater. Today **15**, 266 (2012).
[7] N. Lindahl, D. Midtvedt, J. Svensson, O. A. Nerushev, N. Lindvall, A. Isacsson, and E. E. B. Campbell, Nano Letters **12**, 3526 (2012).
[8] Q. Lu and M. Arroyo Huang, J. Phys. D **42**, 102002 (2009).
[9] J. A. Aronovitz and T. C. Lubensky, Phys. Rev. Lett. **60**, 2634 (1988).
[10] Y. Kantor, M. Kardar, and D. R. Nelson, Phys. Rev. A **35**, 3056 (1987).
[11] W. Helfrich, Z. Naturforsch. C **28**, 693 (1973).
[12] L. D. Landau, L. P. Pitaevskii, E. M. Lifshtz, and A. M. Kosevich, *Theory of Elasticity*, 3rd edition, Vol. 7 (Butterworth-Heinemann, Oxford, UK, 1986).
[13] M. Droth and G. Burkard, Phys. Rev. B **84**, 155404 (2011).
[14] D. L. Nika, S. Ghosh, E. P. Pokatilov, and A. A. Balandin, Appl. Phys. Lett. **94**, 203103 (2009).
[15] S. Costamagna and A. Dobry, Phys. Rev. B **83**, 233401 (2011).
[16] J. H. Los, M. I. Katsnelson, O. V. Yazyev, K. V. Zakharchenko, and A. Fasolino, Phys. Rev. B **80**, 121405 (2009).
[17] R. Roldán, A. Fasolino, K. V. Zakharchenko, and M. I. Katsnelson, Phys. Rev. B **83**, 174104 (2011).
[18] D. L. Nika, A. S. Askerov, and A. A. Balandin, Nano Lett. **12**, 3238 (2012).
[19] N. Bonini, J. Garg, and N. Marzani, Nano Lett. **12**, 2673 (2012).
[20] J. C. Meyer, A. K. Geim, M. I. Katsnelson, K. S. Novoselov, T. J. Booth, and S. Roth, Nature (London) **446**, 60 (2007).
[21] M. M. Fogler, A. H. Castro Neto, and F. Guinea, Phys. Rev. B **81**, 161408(R) (2010).
[22] A. A. Balandin and K. L. Wang, Phys. Rev. B **58**, 1544 (1998).
[23] L. Brey and H. A. Fertig, Phys. Rev. B **73**, 235411 (2006).